ELSEVIER

Polymer 42 (2001) 6945–6959

polymer

www.elsevier.nl/locate/polymer

Block copolymers of polystyrene and side-chain liquid crystalline siloxanes: morphology and thermal properties

Aaron Moment, Paula T. Hammond*

Department of Chemical Engineering, Room 66-550, Massachusetts Institute of Technology, 77 Massachusetts Avenue, Cambridge, MA 02139-4307, USA

Received 28 April 2000; received in revised form 2 February 2001; accepted 5 February 2001

Abstract

Well-defined diblock copolymers of polystyrene and smectic side-chain liquid crystalline siloxanes have been prepared with a wide range of molecular weights (M_n total from 20,000 to 165,000) and liquid crystalline siloxane weight fractions (0.4–0.91). Two different types of block copolymers were examined, each series having a different mesogen attached to the siloxane block. Increasing the rigidity of the mesogen led to stronger microphase segregation between the PS and LCP blocks, and to a higher T_g and LC clearing point for the LCP block. Samples with large LCP weight fractions (>0.8) and low T_g (< − 25°C) LCP blocks were elastomeric at room temperature, presumably because of the high molecular weight of the siloxane block (80–130 K). As the mesogen choice and the block lengths were varied, four general types of morphologies were observed using transmission electron microscopy (TEM) and small angle X-ray scattering (SAXS): hexagonally packed LC cylinders, alternating PS–LCP lamellae, weakly ordered PS cylinders, and hexagonally packed PS cylinders. The PS cylinder morphology persisted to unusually high LCP weight fractions.

Keywords: Liquid crystalline block copolymers; Polystyrene siloxane functional polymers; Liquid crystalline elastomers

1. Introduction

The use of block copolymers has been of great interest for the creation of nanostructured materials, due to the tendency of these polymers to microphase segregate into ordered nanometer sized domains. Molecular scale order within one of the microphases of the block copolymer material can be realized by incorporating a mesogenic (liquid crystalline) block into a diblock copolymer. In this instance, one can influence the ordering of the mesogenic regions of the material by orienting the block copolymer domains, resulting in molecular to nanoscale order. Of particular interest is the ability to introduce the properties of low molar mass liquid crystals, such as electric or magnetic field alignment, into the nanostructure of block copolymers; to achieve this goal, side chain liquid crystalline polymers may be used as a block in an amorphous–liquid crystalline block copolymer. This area has become an active focus of investigation in the past several years [1–10].

The ability to create phase segregated polymeric systems in which a mobile liquid crystalline phase can exist within a rigid, glassy, supporting matrix could provide a route to free standing electro-optical or magneto-optical thin films. Such systems eliminate the need for specific surface treatments to orient LC mesogens, as the block copolymer interface provides the means of orientation [8,11]. Liquid crystalline blocks exhibiting the smectic C^* phase are of particular interest [8,11] as the block copolymer morphology can be used to stabilize the ferroelectric smectic C^* phase [12]. An added advantage is the expected improved stability to mechanical shock and potential benefit in increased toughness and durability of LC devices, a problem of particular interest in the manufacture of ferroelectric LC displays.

Finally, a number of traditional triblock and segmented copolymers exhibit elastomeric mechanical properties. Covalently crosslinked liquid crystalline siloxane networks have been studied extensively [13,14], and continue to receive attention [15] as they show promise as piezo-elements [16] and mechano-optical systems. The incorporation of side chain mesogens within a phase segregated thermoplastic elastomer matrix should produce liquid crystalline thermoplastic elastomers (LCTPE's) with unique mechano-optical properties, which can be fine tuned or dramatically altered with changes in processing, degree of orientation, and morphology. If a ferroelectric mesogen is chosen, it should be possible to observe a coupling between electrical polarization and mechanical deformation; this sort

* Corresponding author. Tel.: +1-617-258-7577; fax: +1-617-258-5766.
E-mail address: hammond@mit.edu (P.T. Hammond).

0032-3861/01/$ - see front matter
PII: S0032-3861(01)00115-X

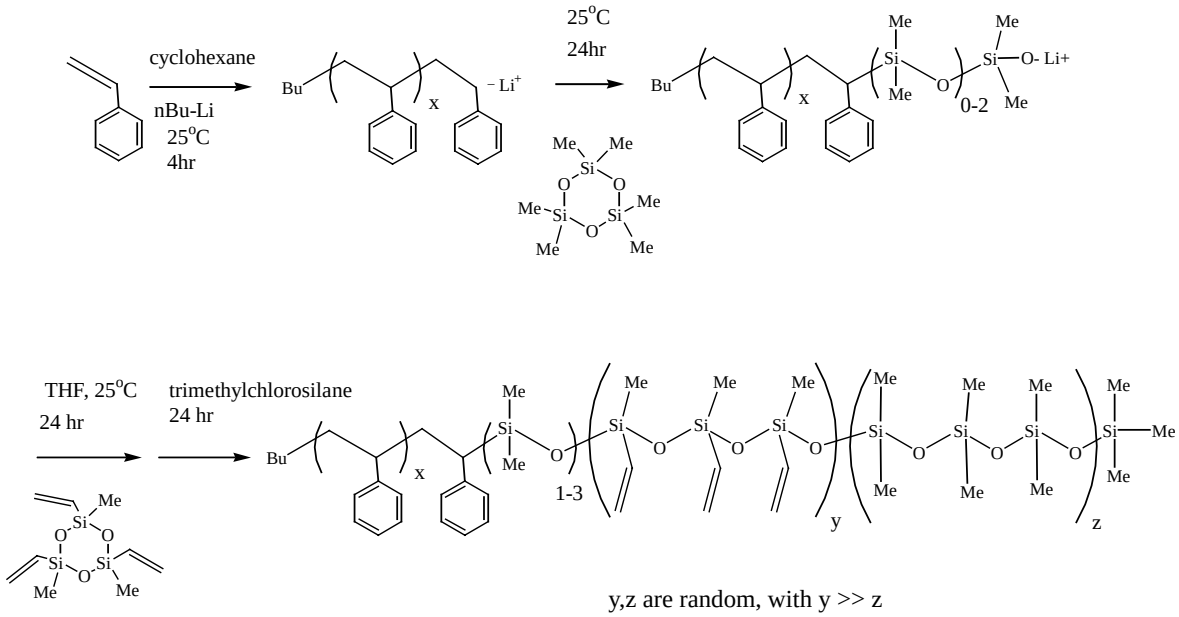

Fig. 1. Anionic synthesis of a PS–PVMS backbone. Living polystyrene is prepared in cylcohexane at room temperature using Bu–Li as an initiator. The reactivity of the living polystyrl anion is reduced by the addition of D3, and the vinyl functional V3 monomer is added with THF, which acts as a polymerization promoter. Finally, the diblock copolymer is end-capped with trimethylchlorosilane.

of piezoelectric effect may provide a route to new electromechanical or electrical field induced damping systems in well aligned samples.

The development of such LCTPEs and responsive LC multisegmented copolymers has been a goal in our research group; the design of systems in which one block is rigid and glassy, and the second liquid crystalline block is fluid and well above the glass transition temperature (while remaining below the LC clearing point) is critical to this goal. Because of their low T_g, the field dependent properties of liquid crystalline siloxane homopolymers, such as electro-optic switching, may be accessed at room temperature [17–20]. We have recently developed a method for the synthesis of diblock copolymers of polystyrene and functionalized side-chain liquid crystalline siloxanes [21], which comprise the first block copolymers to contain rigid blocks alternating with flexible liquid crystalline blocks; the materials addressed in this paper are the diblock copolymers shown in Fig. 1. This work is also unique in its use of polysiloxanes, resulting in the lowest T_gs (approx. −30°C) of any of the reported ferroelectric liquid crystalline blocks incorporated into block copolymers. Narrow molecular weight distribution side-chain liquid crystalline siloxane based homopolymers have only recently been synthesized anionically, using methods developed in our labs [21] concurrently with other researchers [22]. By incorporating these anionic liquid crystalline siloxanes into block copolymers with polystyrene, a wide range of morphologies and properties become possible. Increasing the volume fraction of liquid crystal block, for example, changes the mechanical properties from hard and brittle to pliant and elastomeric. Extension of the diblock system described here to PS–LCP–PS triblocks should give true liquid crystalline elastomers with non-covalent crosslinks. In this paper, the physical properties and morphology of polystyrene–LC siloxane diblock polymers will be discussed. As expected, the block lengths, block volume fractions, and the mesogen choice were all found to influence the physical properties, the morphology, and the phase segregation of the polymer. In particular, we found that the length, rigidity and chemical structure of the mesogen can greatly influence the extent of phase segregation, the nature of the block copolymer interface, and the stability of the resulting LC phase.

2. Experimental

2.1. Synthesis

The synthetic approach to the PS–LCP block copolymers, which has been described in a separate publication [21], is to first prepare a polystyrene–polyvinylmethylsiloxane (PS–PVMS) block copolymer using sequential anionic polymerization of styrene and cyclic siloxanes (Fig. 1), and then to attach Si–H functional mesogens to the siloxane block via hydrosilyaltion chemistry (Fig. 2). The anionic synthesis used here is a variation of one of the first PS–PDMS schemes published in 1970 [23]. The key to our

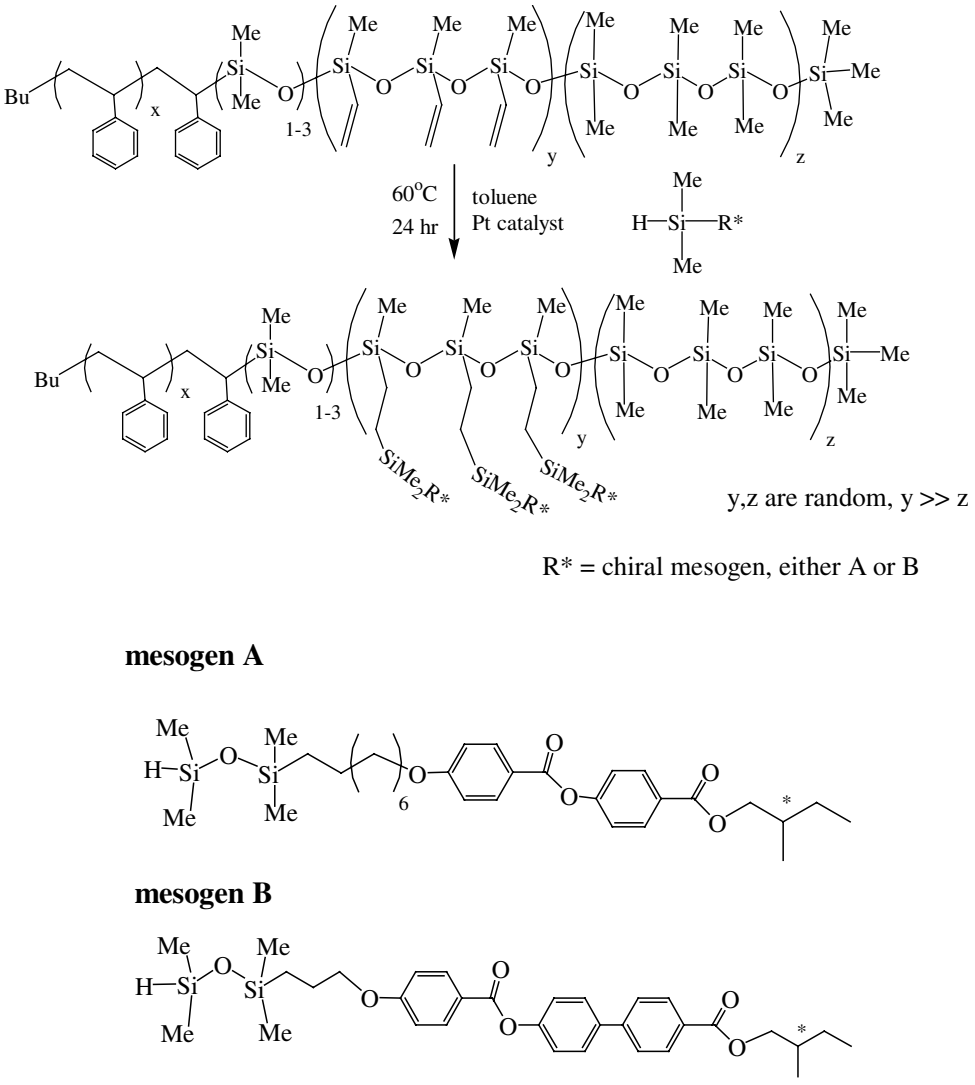

Fig. 2. Structures of Si–H functional mesogen A and mesogen B and their attachment to a PS-PVMS backbone. Mesogen B has a more rigid core and a shorter spacer than mesogen A.

technique is reducing the reactivity of the living polystyrl anion prior to the addition of the cyclic V3 monomer, which contains three vinyl groups that are susceptible to attack by the living polystyrene. This reduction in reactivity was accomplished by the addition of the cyclic trimer D3, which converts the living polystyrl anion into the less reactive lithium siloxanolate anion. The lithium siloxanolate can then safely initiate the V3 monomer, and THF is added as a polymerization promoter (Fig. 1). Strictly speaking, the polymers made this way are triblock copolymers, with a very small 'block' of D (dimethyl) units (between one and three units) followed by a block containing V3 units. A small amount of remaining D3 present in the reaction solution will become incorporated into the V3 block in small quantities (approximately 1:50 to 1:100 ratio of D3 to V3). This is illustrated schematically in Fig. 1.

After isolating the PS–PVMS block copolymers, mesogens containing a Si–H functional end-group were attached to the PVMS block via hydrosilylation chemistry (Fig. 2). The crude product was then precipitated 2–3 times from THF into methanol (mesogen A polymers) or ethanol (mesogen B polymers) until no mesogen remained as measured by thin layer chromatography (TLC) and GPC. The mesogens were prepared by funtionalizing vinyl terminated precursor with an excess of dimethylsiloxane (Fig. 3). In addition to the block copolymers, functionalized LCP homopolymers were prepared by the anionic polymerization of V3 initiated by lithium trimethylsiloxanolate, followed by a mesogen attachment step to the siloxane homopolymer. These homopolymers provide a useful reference point to compare with the block copolymers.

The two mesogens used in this study, (*S*)-2-methylbutyl 4-[4-(8-(1,1,3,3 tetramethyldisiloxane)octanyloxy)benzoyloxy]benzoate and (*S*)-2-methylbutyl 4-[4-(3-(1,1,3,3 tetramethyldisiloxane)propanyloxy)benzoyloxy]biphenylbenzoate, denoted A and B, respectively, are shown in Fig. 2. An

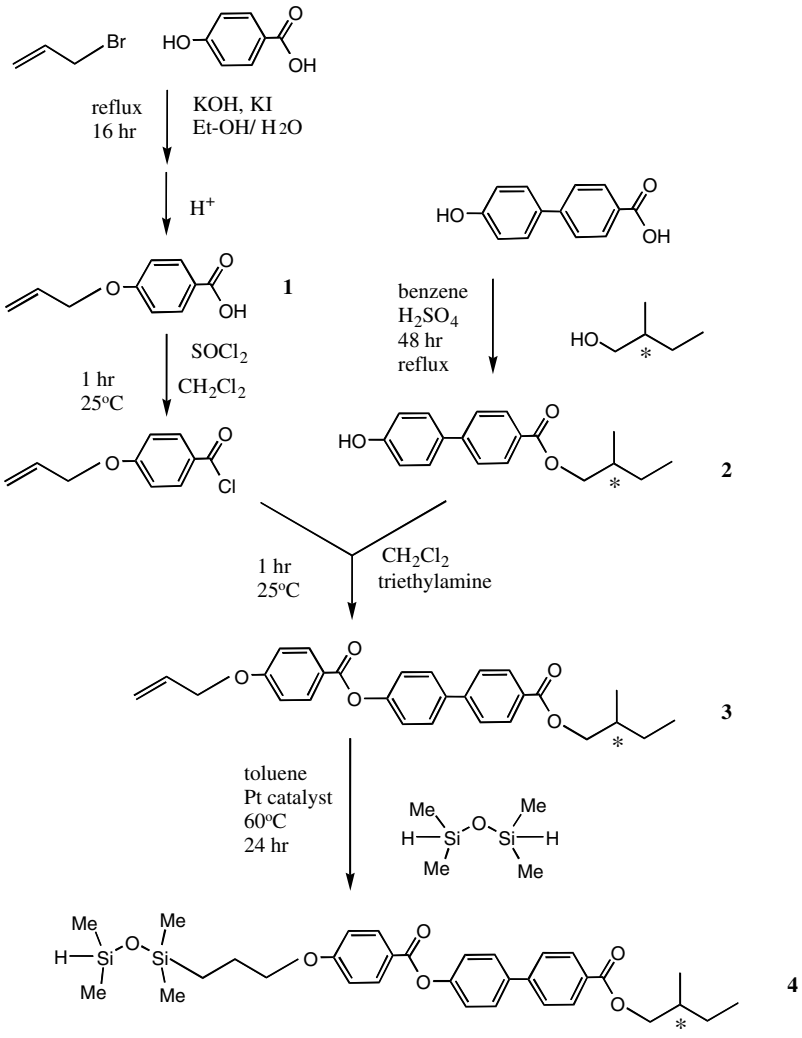

Fig. 3. Synthesis of Si–H mesogen B. The final step is the conversion of a vinyl terminal mesogen to an Si–H terminal mesogen by reaction with excess 1,1,3,3 tetramethyldisiloxane.

inherent problem with the initial synthetic technique is variability in the degree of substitution of mesogen A along the PVMS backbone, with values ranging from 72 to 100% for similar reaction conditions. This problem was addressed for the mesogen B series by increasing the reaction times from 1–2 days to 4 days, and resulted in nearly complete substitution of the mesogen along the polymer backbone for the block copolymer samples, and 82% substitution for the homopolymer case. Mesogen B was synthesized as described below and in Fig. 3, using a scheme similar to that used for mesogen A.

2.2. Synthesis of mesogen B

2.2.1. 4-(3-Propenyloxy)benzoic acid (1)

34.53 g (0.25 mol), of 4-hydroxybenzoic acid was added to a solution containing 175 ml ethanol, 28.05 g (0.5 mol) KOH, 2.12 g of KI, and 35 ml of water. 30.25 g (0.25 mol) 3-bromo-1-propene was then added to the mixture through an addition funnel. The solution was refluxed for 18 h, cooled to room temperature, diluted with 300 ml water, and then acidified to pH 4 with HCl. The white precipitate was washed thoroughly with water and recrystallized once from ethanol. 23.0 g of white crystals were obtained, 51.7% yield.

2.2.2. (S)-2-Methylbutyl 4-hydroxybiphenyl-4-carboxylate (2)

75 ml benzene, 10 g (0.110 mol) (*S*)-2-methyl-1-butanol, 8.14 g (0.038 mol) 4-hydroxy-4-biphenyl carboxylic acid, and 0.5 ml of concentrated sulfuric acid were added to a round bottom flask fitted with a Dean–Stark condenser. The reaction mixture was refluxed for 60 h and then cooled to room temperature. After removing the benzene with a rotary evaporator, the crude solid product was recrystallized two times from a 1:1 (v/v) toluene/hexane mixture. 10.79 g of white crystalline solids were recovered, 76% yield.

2.2.3. (S)-2-methylbutyl 4-(4-(3-propenyloxybenzoyloxy)) biphenyl-4-carboxylate (3)

3.93 g (0.022 mol) 4-(3-propenyloxy)benzoic acid, three drops DMF, and 4.81 ml thionyl chloride (0.066 mol) were added to a flask with stirring. The reaction was stirred at room temperature for 30 min before removing the excess thionyl chloride on a vacuum line, leaving behind the acid chloride. In a separate flask, 6.26 g (0.022 mol) of (**2**) and 6 ml (0.043 mol) triethylamine were dissolved in 25 ml methylene chloride. The acid chloride was diluted with methylene chloride and added dropwise to the flask containing (**2**). HCl gas emanated from the reaction mixture immediately upon the addition of the acid chloride solution. After stirring overnight at room temperature the reaction mixture was washed with water three times. The solvent was then removed by a rotary evaporator and the crude product recrystallized from ethanol. 8.25 g of white crystalline solids were recovered, 84.5% yield.

^{1}H NMR: $\delta = 0.98$–1.07 (m, 6 aliphatic, $-CH_3$), 1.32–1.35 (m, 1 aliphatic H), 1.56–1.61 (m, 1 aliphatic H), 1.90 (m, 1 aliphatic H), 4.19–4.26 (m, 2H, CH_2OCOPh), 4.66 (d, 2H, CH_2=CH–CH_2–OPh), 5.38–5.40 (m, 2H, CH_2=CH–), 6.05–6.12 (m, 1H, CH_2=CH–), 7.03–7.05 (m, 2H, Ar–H), 7.32–7.34 (m, 2H, Ar–H), 7.68–7.70 (m, 4H, Ar–H), 8.14–8.21 (m, 4H, Ar–H).

2.2.4. (S)-2-methylbutyl 4-[4-(3-(1,1,3,3 tetramethyl disiloxane)propanyloxy)benzoyloxy]biphenylbenzoate (4, final Si–H tipped mesogen B)

1.52 g (2.62 mmol) of vinyl mesogen (**3**) was dissolved in a minimal quantity of toluene (12 ml) and mixed with six drops of a platinum catalyst in xylenes (platinum–divinyl tetramethyl disiloxane complex in xylenes, Gelest product: SIP6831.0) In a separate flask, 7 ml (39.5 mmol) tetramethyldisolxane and 4 ml toluene were brought to 60°C under N_2 with stirring. The solution of catalyst and (**3**) was then added dropwise to the disilane mixture over the course of 12 min. The reaction was easily monitored by TLC (10:1 (v/v) hexane/ethyl acetate solvent system). After 18 h, all the starting material had been consumed, and the excess solvent and disilane was removed by vacuum (0.1 mmHg) for 4 h, leaving behind a yellow cake of solids. The crude solids were easily soluble in a 10:1 hexane/ethyl acetate mixture. Silica gel chromatography (6 column) in 10:1 hexane ethyl acetate yielded 0.92 g of white solids, 47% yield. The presence of the Si–H bond was confirmed by NMR and by FT-IR (strong Si–H peak at 2121 cm^{-1}). ^{1}H NMR: $\delta = 0.09$–0.22 (m, 12H, Si–CH_3), 0.70–0.71 (m, 2H, RCH_2–Si) 0.98–1.07 (m, 6 aliphatic $-CH_3$), 1.32–1.35 (m, 1 aliphatic H), 1.50–1.62 (m, 1 aliphatic H), 1.80–2.1 (m, 3H, aliphatic H), 4.03–4.06 (m, 2H, CH_2OPh). 4.19–4.26 (m, 2H, CH_2OCOPh), 4.73 (s, 1H, Si–H), 7.03–7.05 (m, 2H, Ar–H), 7.32–7.34 (m, 2H, Ar–H), 7.68–7.70 (m, 4H, Ar–H), 8.14–8.21 (m, 4H, Ar–H) FTIR: strong Si–H stretch at 2121 cm^{-1}.

2.3. Characterization

Sample preparation. All polymer samples were cast from concentrated (~10 wt%) toluene solutions onto teflon coated sheets and then air dried for ~24 h. The films were then vacuum dried for ~18 h at elevated temperature prior to SAXS and TEM measurements. Annealing temperatures were selected (80–110°C) to be above or at the polystyrene T_g, and below the LC clearing point when possible. In all cases, the LCP T_g was below room temperature. Films of the solvent cast samples were on the order of 0.25 mm thick.

TEM. A Reichert–Jung FC4E Ultracut E was used to ultracryomicrotome samples below room temperature. The diamond knife temperature was set at −100°C and the sample temperature set at −120°C. Films of thickness 30–60 nm were transferred to copper grids and stained for 15 min with the vapor from a RuO_4 0.5% aqueous solution. Samples were then observed with a JEOL 200CX electron microscope operating at 200 kV. The RuO_4 selectively stains the polystyrene domains, making them appear dark in the TEM images.

SAXS. A Seimens 2-D SAXS detector placed 64 cm from the sample was used to detect the scattering of Cu Kα X-rays at 40 kV and 24 mA. For temperature-controlled studies, the sample was placed in a hot stage (Instec, model HS250) equipped with a temperature controller (Instec, model STC200). Temperatures as high as 250°C were possible with an accuracy of ±0.4°C.

DSC. A Perkin–Elmer DSC-7 with a liquid nitrogen cooling system was used for low temperature DSC. All scans were conducted at a heating/ cooling rate of 20°C min^{-1}, and the final results were taken from the second or third heating scan.

OM. A Lieca Optical Microscope equipped with a Mettler FP82HT hot stage/FP90 controller was used to observe samples under crossed polarizers at different temperatures.

GPC. A Waters gel permeation chromatography (GPC) system equipped with with two Styragel HT3 columns (500–30,000 MW range), one Styragel HT4 column (5000–600,000 MW range), and a UV detector (254 nm) was used for molecular weight measurement relative to polystyrene standards. Tetrahydrofuran (THF) flowing at 1 ml min^{-1} was the mobile phase.

NMR. ^{1}H NMR measurements were taken with a Bruker Avance DPX400 400 MHz instrument using $CDCl_3$ as a solvent. The relaxation time D1 was set to 15 s in order to improve the accuracy of peak integrations.

3. Results and discussion

3.1. Structural characterization

Tables 1–4 summarize the block copolymer and homopolymer structures synthesized with both mesogens, and illustrate the wide range of molecular weights that have

Table 1
Molecular weight characterization of polymers made w/meosgen A

Samples	Wt % LCP	M_n, PS GPC	M_n, siloxane GPC	M_n, siloxane NMR	% sub NMR	M_n, LCP NMR	M_n, LCP GPC
LC homopolymer							
LCPA 48	100	–	6900	–	92	48,200	34,500
Block copolymers							
PS 12–LCPA 8	41	12,000	2600	1500	100	8200	15,900
PS 39–LCPA 30	44	39,300	7600	5700	82	30,300	21,800
PS 13–LCPA 82	86	13,300	27,400	16,100	73	82,500	38,100
PS 14–LCPA 132	90	14,100	29,100	21,200	86	132,200	57,000

Table 2
Polydispersity index of polymers made w/mesogen A

Samples	Wt % LCP	PS block PDI	PS–PVMS PDI	PS–LCP PDI (after mesogen added)	% substitution NMR
LC homopolymer					
LCPA 48	100	–	1.22	1.26	92
Block copolymers					
PS 12–LCPA 8	41	1.03	1.05	1.18	100
PS 39–LCPA 30	44	1.02	1.04	1.42	82
PS 13–LCPA 82	86	1.05	1.13	1.49	73
PS 14–LCPA 132	90	1.06	1.13	1.32	86

Table 3
Molecular weight characterization of polymers made w/mesogen B

Samples	Wt % LCP	M_n, PS GPC	M_n, siloxane GPC	M_n, siloxane NMR	% sub NMR	M_n, LCP NMR	M_n, LCP GPC
LC homopolymer							
LCPB 47	100	0	10,300	–	82	47,300	30,437
Block copolymers							
PS 12–LCPB 8	41	12,000	2600	1500	99	8300	18,400
PS 14–LCPB 151	91	14,100	29,100	21,200	99	151,200	87,400

Table 4
Polydispersity index of polymers made with mesogen B

Samples	Wt % LCP	PS block PDI	PS–PVMS PDI	PS–LCP PDI (after mesogen added)	% substitution NMR
LC homopolymer					
LCPB 47	100	–	1.29	1.41	82
Block copolymers					
PS 12–LCPB 8	40	1.03	1.05	1.20	99
PS 14–LCPB 151	91	1.06	1.13	1.23	99

been made. There were no apparent practical limits on LCP block sizes; large (~150,000 M_n) and small (~8000 M_n) LCP blocks were prepared. Samples are labeled by the molecular weights of each block and the mesogen used, either A or B. Thus, PS 12–LCPA 8 is a block copolymer sample with the following structure: polystyrene $M_n = 12,000$; liquid crystalline siloxane (mesogen A) $M_n = 8000$. The same system is used to label homopolymers, e.g. LCPB 47 is a liquid crystalline siloxane homopolymer (mesogen B) with M_n 47,000. The LCP block molecular weight in the sample label is an estimate from NMR integration, as this proved to be most accurate in light of our morphological characterization.

The polydispersities of each polymer and its precursors are tabulated in Tables 2 and 4. The PDI increases as the synthesis progresses from PS block to PS–PVMS block

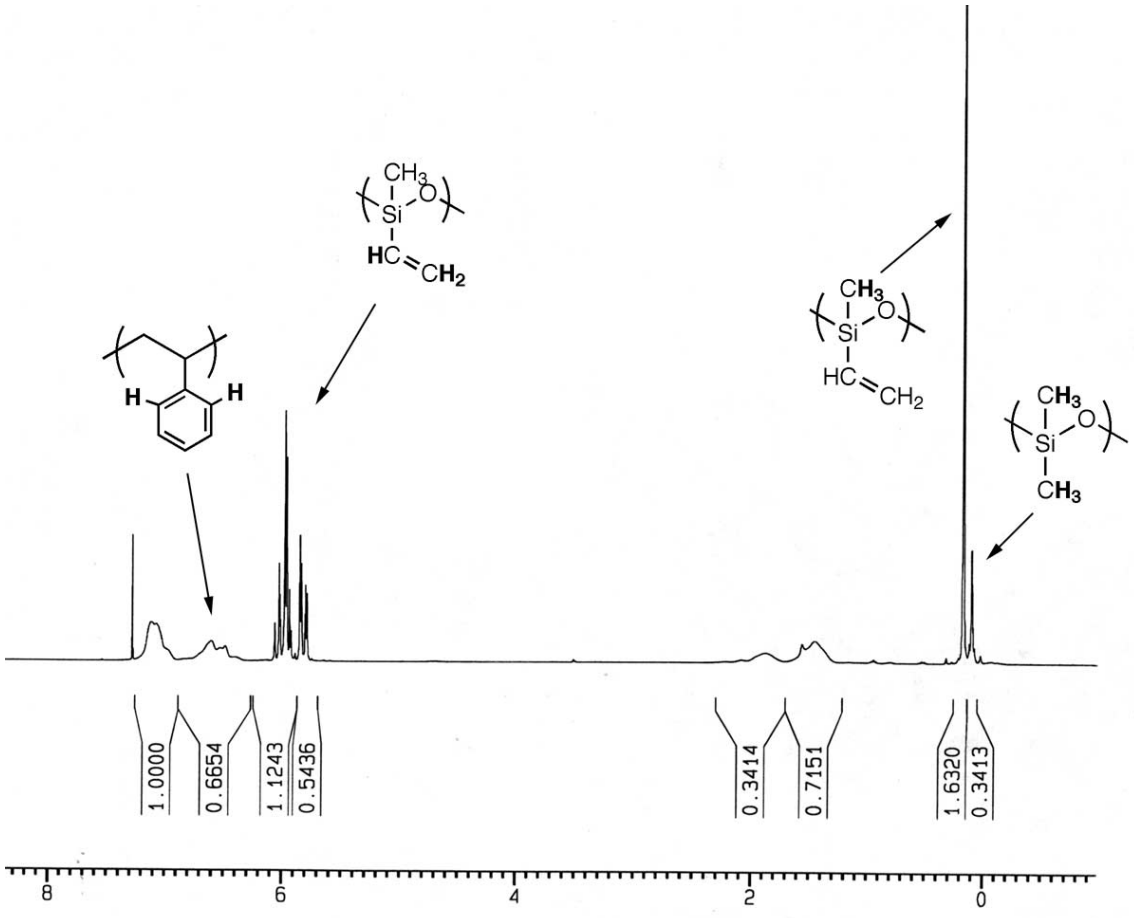

Fig. 4. ^{1}H NMR of PS–PVMS substrate prior mesogen addition, illustrating the three repeat units that are considered in determining the composition and molecular weight of the siloxane block prior to functionalization with Si–H mesogens.

copolymer and finally to the functionalized PS–LCP. The anionically polymerized PS blocks have PDI $\leq$1.06; after the siloxane blocks have been polymerized, the resulting block copolymers have PDI $\leq$1.13. This increase in PDI is due to the anionic ring-opening siloxane polymerization, which is living, but results in PDIs slightly higher [21,22,24] than those observed in more conventional anionic polymerizations. This is due to back-biting and other redistribution reactions that are possible in all siloxane systems in the presence of a basic anionic initiator [24,25]. After the mesogens are attached there is a final rise in PDI, with larger increases observed for lower degrees of substitution. The final PS–LCP block copolymers have PDI $\leq$1.49, lower than most siloxane homopolymers reported in the literature, and low enough to display well ordered microphase segregated structures, as we demonstrate in SAXS and TEM.

The molecular weight of the polystyrene block was estimated by taking a GPC of this block before the siloxane block was polymerized. Because our GPC is calibrated with respect to polystyrene standards, the polystyrene block MW is known accurately.

The molecular weight estimates of the LCP block were obtained from NMR integration. We chose NMR instead of GPC estimates because the NMR results are based on a final chemical structure, rather than a comparative approach with PS standards.

After the siloxane monomers were added and polymerized, ^{1}H NMR integration was used to calculate the composition of the resulting PS-PVMS polymer. Because D3 monomer is used to convert the living polystyryl anion to a siloxanolate anion before the addition of V3 (Fig. 1), the siloxane block contains both methylvinyl siloxane repeats and dimethyl siloxane repeat units. Three types of repeat units are therefore considered: polystyrene repeats, polydimethyl siloxane repeats, and vinylmethyl siloxane peaks. Each of these units has distinct peaks in NMR as shown in Fig. 4. The composition of the PS–PVMS block copolymer is estimated from these peaks. The PS molecular weight (GPC) and the composition of the PS–PVMS block copolymer (NMR) are then used to calculate a molecular weight of the siloxane block, and the average number of vinyl repeats in the siloxane block. In addition, the ratio of vinyl units to styrene units is noted, as the vinyl groups are subsequently reacted to form covalent linkages to the mesgoens. This ratio is taken as 2/3 times the vinyl proton integration divided by the integration of the two meta

Table 5
T_gs and smectic clearing points of polymers made w/mesogen A. Thermal transitions are taken from the second or third heating scan at 20°C min^{-1}

Sample ID	Wt % LCP	PS T_g°C	LCP T_g°C	Smectic clearing Pt. °C	ΔH clearing J g^{-1} LCP
LCPA 48	100	–	− 24	90	6.71
PS 12–LCPA 8	41	–	–	–	–
PS 39–LCPA 30	44	84	− 35	43	0.39
PS 13–LCPA 82	86	70	− 34	60	4.01
PS 14–LCPA 132	90	61	− 32	79	6.20

aromatic polystyrene protons (δ 6.60–6.49 ppm). These two aromatic protons were selected because they do not overlap with any of the mesogen protons. Moreover, these protons do not significantly overlap with the three other aromatic PS protons, as evidenced by clean integration (2:3). Once the mesogen has been attached to the second block and the polymer purified, NMR of this product gives the ratio of remaining vinyl units to polystyrene units. Since the number of polystyrene units remains the same before and after the mesogen is attached, a degree of substitution can be calculated, that is the fraction of vinyl groups that have reacted with the mesogen. The molecular weight of the entire LCP block is taken as the sum of the siloxane block M_n before mesogen attachment and the additional molecular weight due to the added mesogens. This is reported as an NMR based number average molecular weight estimate for the LCP block in Tables 1 and 3.

For samples with large LCP blocks (NMR block size >50K), the GPC estimate is significantly smaller than the NMR estimate, the extreme case being PS 14-LCPA 132, in which the NMR estimated LCP M_n is 132,000, while the GPC estimate is 57,000. This trend is in agreement with the common observation that branched polymers have intrinsic viscosities lower than linear molecules of the same molecular weight [26]. The LCP blocks can be considered a type of branched polymer; as the LCP M_n increases, the coil size does not increase proportionally, and hence the GPC estimates will underpredict the M_n. For small LCP blocks (NMR block size <10K), the opposite situation is observed, so that the NMR M_n is significantly smaller than the GPC estimate. This is probably due to a high persistence length of the LC block at low MWs, a situation where a true random coil is not the best model.

3.2. Mesogen A polymers: LC phase behavior and morphology

The samples functionalized with mesogen A range in total molecular weight from 20,000 to 146,000 with weight fractions of liquid crystal from 0.4–0.90, as shown in Table 1.

Thermal transitions of each polymer were monitored using DSC and OM; these results are shown in Table 5. SAXS diffractograms of the homopolymer and block copolymers indicate a smectic layer peak with periodicity of 3.6 nm. Previous literature with similar mesogens attached to siloxane backbones indicates a smectic C* phase [17,18]. Bistable switching experiments of the homopolymer indicate a smectic C*, so it is likely that a smectic C* phase is also present in the block copolymer; however X-ray scattering was performed on samples that were not macroscopically oriented, making it difficult to ascertain smectic C vs. A arrangements. The X-ray reflection at small angles in both homo- and block copolymers confirms the presence of a disordered smectic phase. The 3.6 nm spacing is close to the spacing given by molecular modeling of mesogen A (using MOPAC), which yields a mesogen size of 3.1 nm at the lowest energy. The OM observations of the polymers were of sandy, fine grained smectic textures. In addition, the same smectic spacing of ~3.6 nm was maintained in all the LC block copolymers and homopolymers.

The lowest molecular weight sample, PS 12-LCPA 8, had no observable T_gs or clearing points, nor was it birefringent in OM. In addition, this sample had no smectic or morphological SAXS peak; thus, we conclude that the blocks in PS 12–LCPA 8 are phase mixed due to their low molecular weight. All other block copolymer samples in this series have two distinct T_gs and a single liquid crystalline transition, a smectic clearing point. For illustration, Fig. 5 contains a DSC scan showing the two T_gs and the single liquid crystalline clearing point of sample PS 14-LCPA 132.

As the polystyrene content increases in this series, the liquid crystalline clearing point decreases from 90°C in the homopolymer to 43°C in PS 39-LCPA 30. In addition, the polystyrene T_g is plasticized by the LC block by as much as 30°C in PS 14-LCPA 132. These trends suggest a considerable degree of phase mixing which destabilizes (lowers the clearing point) the LCP phase and plasticizes the polystyrene. The clearing point enthalpies for mesogen A polymers normalized per gram of LCP also decrease with increasing PS content. Above 50% LC volume fraction, when the LC forms the continuous matrix, the enthalpies are much closer to that of the original homopolymer.

A drop in normalized clearing enthalpy relative to the LC homopolymer is a common but not universal [8] observation in amorphous–LCP block copolymers [1,5,9,27,28]. This observation may be due to a destabilization of the LC phase at or near the block interface due to unfavorable anchoring effects or to the presence of a fairly diffuse disordered interfacial region w/ poorly ordered LCP. Disordered LCP in the interfacial area between the domains reduces the mass of actual liquid crystalline material involved in the thermal transition.

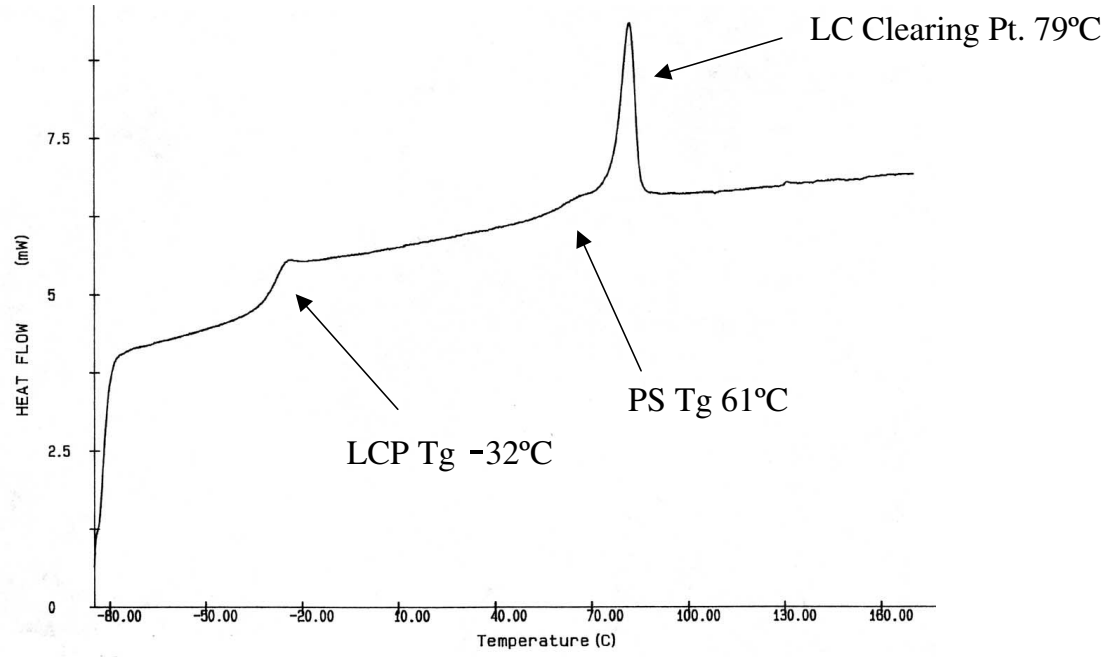

Fig. 5. DSC heating scan at 20°C^{-1} of PS 14–LCPA 132, showing two T_gs and a single liquid crystalline clearing point.

Clearing point temperature trends in amorphous-LCP block copolymers are more difficult to assess, as both clearing point elevation [29] and depression [9,30] have been observed, in addition to the observation of little to no change in clearing point relative to similarly sized LCP homopolymers [1,5]. These systems all differ in their mesogen choice, which implies that transition temperature trends are probably linked to enthalpic effects of mesogen anchoring at the interface. In the case of mesogen A copolymers the most likely reason for the clearing point depression is phase mixing phenomena, as there is evidence in TEM and DSC data (i.e. plasticization of polystyrene). Other issues such as the morphology and molecular weight could influence the clearing point, but these are not dominant factors. In fact, the T_g is lower in all of the block copolymers with mesogen A than it is in the lower molecular weight mesogen A homopolymer. In general, reports of other LC block copolymer systems from this group and other researchers also indicate little correlation between the LC clearing point and domain morphology.

In polystyrene–polymethacrylate side chain liquid crystalline block copolymers [7], the polystyrene block stabilized the smectic C* phase in lamellar samples (at the expense of a cholesteric phase) relative to the homopolymer, and the clearing points were stabilized by as much as 20°C with respect to the LC homopolymer.

On the other hand, Mao et al. observed a clearing point depression of ~20°C in lamellar samples; when the morphology shifted to LC cylinders the clearing point then rose to 3°C higher than the LC homopolymer [9]. This system was strongly segregated and did not show signs of phase mixing, hence the depression in clearing point is related to interface/ packing effects and not to mixing. In the PS–LCPA siloxanes presented in this paper, the combination of phase mixing and interface destabilization likely exaggerates these trends relative to other systems and results in a severe clearing point depression in the lamellar sample PS 39–LCPA 30. Both samples PS 13–LCPA 82 and PS 14–LCPA 132 have a similar morphology of weakly ordered polystyrene cylinders; the difference in clearing point transition between these samples is likely linked to the fact that phase segregation is stronger for the higher molecular weight block copolymer.

The third column of Table 6 shows SAXS measurements of the smectic layer spacing in the PS–LCPA siloxane samples, which do not change more than an angstrom (relative to a pure LC homopolymer). The interfacial region and the polystyrene domains probably contain some isotropic LCP, as evidenced by the plasiticized polystyrene domains as well as by a clearing point depression and lowered isotropization enthalpies.

When initially cast from toluene and dried, all the samples in the mesogen A series showed diffuse SAXS scattering from 10–50 nm, and the liquid crystalline samples had a clear smectic peak at 3.6 nm. The samples were then annealed and SAXS traces measured again. TEM was conducted on the annealed samples if a significant increase in morphological order occurred on annealing, as evidenced by stronger SAXS scattering; otherwise TEM was conducted on the solvent cast samples (to avoid slight discoloration of the samples which occurred during the annealing process and is due to residual platinum catalyst from the synthesis).

In the case of PS 39–LCPA 30, a strong SAXS peak appeared after annealing at 80°C for 12 h. This temperature

Table 6
SAXS peaks and TEM observations of polymers made w/mesogen A

Sample ID	Wt % LCP	SAXS smectic *d* spacing (nm)	SAXS morphology spacing (nm)	TEM morphology spacing (nm)
LCPA 48	100	3.7	–	–
PS 12–LCPA 8	40	–	–	–
PS 39–LCPA 30	43	3.6	28.6	Lamellae, 23.8
PS 13–LCPA 82	86	3.6	Not observed	PS cylinders, 27.5
PS 14–LCPA 132	90	3.6	27.9, weak shoulder	PS cylinders, 22.6

is close to the T_g of the PS in this sample and is well above the LC clearing point of 43°C. The TEM image of this polymer sample (Fig. 6) shows well-ordered alternating lamellae of PS (dark due to RuO_4 staining) and LCP (light). An interesting feature of this TEM image of PS 39–LCPA 30 is the three areas of contrast present in the film. It appears as if the stain is preferentially adsorbed at the interface between the two blocks in a region approximately 2.0 nm in width. One can postulate many reasons for these three areas of contrast; for example, a kinetic staining effect in which the interface is stained first, or a high concentration of unreacted vinyl groups at the interface may result in darker regions at the interface. In addition, the polymers are in fact triblock copolymers with a very small middle block (see Fig. 1), which may also account for the three areas of contrast (although the middle segment of PDMS would not ordinarily be stained by ruthenium tetroxide). One possible explanation for preferential staining of the interface may be due to the presence of disordered LC at the block copolymer interface, which constitutes a large portion of this particular block copolymer based on enthalpy measurements. The ruthenium tetroxide stains aromatic rings in both blocks, but permeates much more quickly to the amorphous polystyrene block than the ordered smectic LC block. On the other hand, without the presence of the ordered smectic phase, it is should be much easier for the stain to permeate, and it is expected that the disordered LC phase would actually be darker than the polystyrene regions due to its high density of aromatic groups.

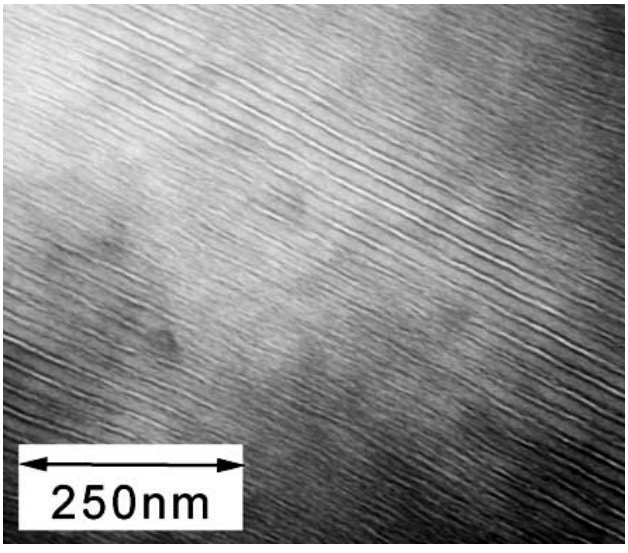

Fig. 6. TEM image of LC PS 39–LCPA 30 showing alternating layers of LCP and PS. The PS regions appear dark due to the RuO_4 stain, which is preferentially absorbed at the interfaces. From this image, the widths of the domains are estimated as follows: PS layer ~16.0 nm, LCP layer ~6.0 nm, and the interfacial region ~2.0 nm.

Another feature of this image is the asymmetry between the domain widths, with the PS domain having an area fraction of ~67%, as measured directly from the TEM image. This value is higher than the 56% area fraction predicted from MW, and may be due to inaccuracies in MW estimation or to staining effects. TEM micrographs of polystyrene–methacrylate based LC block copolymers have also shown similar discrepancies between volume fraction and morphology, and the relative domain size of the polystyrene block for stained samples.

The last two samples, PS 13–LCPA 82 and PS 14–LCPA 132 have a morphology of weakly ordered polystyrene cylinders in a matrix of liquid crystalline polymer. Annealing treatments at a series of temperatures between 60°C and 110°C did not cause significant increases in morphological (relative to solvent cast samples) order as measured by SAXS traces. Fig. 7 shows a TEM image of PS 14–LCPA 132; similar results were obtained for PS 13–LCPA 82. Because these cylinders are not strongly ordered, the SAXS scattering lacks distinct Bragg reflections, and instead shows diffuse scattering, with a shoulder that corresponds to weak first order reflections, shown in Fig. 7. Another reason for the weak scattering could be small electron density differences between the microphases.

The lamellar sample, PS 39–LCPA 30, is well ordered over a long range, while the cylindrical samples, PS 13–LCPA 82 and PS 14–LCPA 132, are not. One possible explanation for our observations is that the lamellar sample is simply more strongly segregated (i.e. further above the phase line in the phase diagram), while the weakly ordered cylindrical samples lie closer to the boundary between miscible blocks and microphase segregation.

The physical properties of all these polymers correlate well with TEM observations; samples with polystyrene cylinders embedded in a continuous soft liquid crystalline siloxane matrix were soft and rubbery, and samples consisting of alternating layers of polystyrene and liquid crystalline siloxane were rigid and glassy. The two PS cylindrical samples, PS 13–LCPA 82 and PS 14–LCPA 132, are

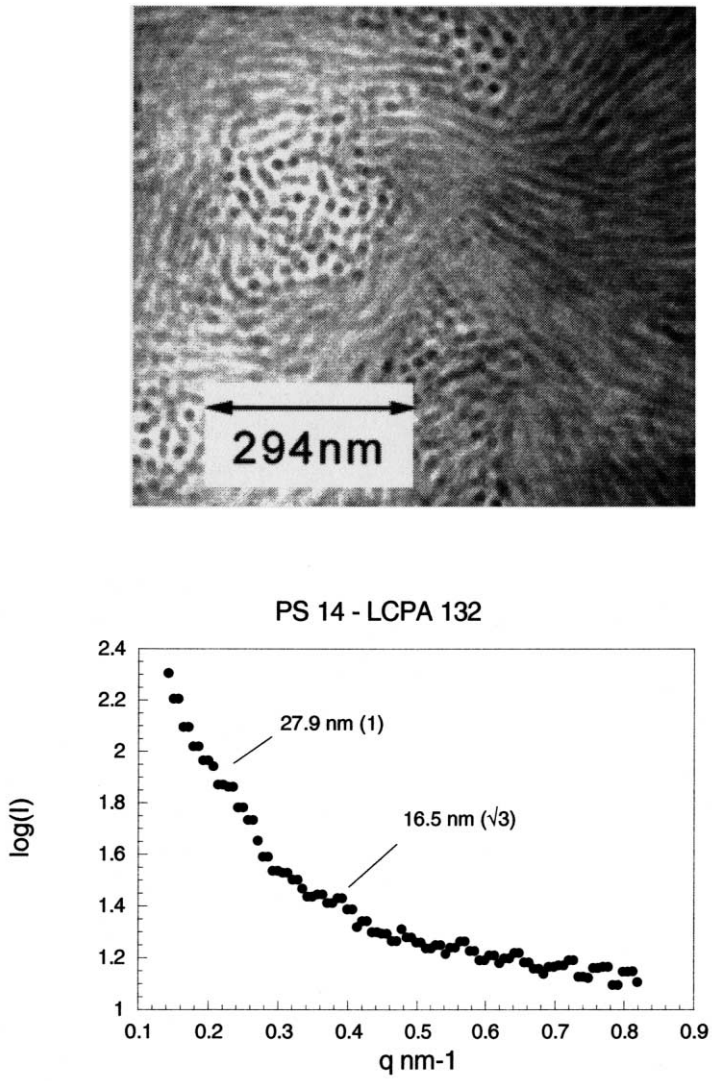

Fig. 7. TEM image and 1-D SAXS plot of sample PS 14–LCPA 132. The weakly ordered PS cylinders result in a SAXS pattern which contains shoulders instead of distinct peaks.

elastomeric in nature; when stretched, they retract back to their original dimensions. These copolymers break at ~40% strain, and exhibit fully recoverable deformation to 8–10% strain. The reversible deformation behavior of these samples is likely due to the combination of a low T_g (~−30°C) and large molecular weight of the liquid crystalline block (80,000–120,000); the polystyrene blocks act as physical elements which add mechanical integrity and toughness.

We are currently studying the mechanical and mechano-optical properties of the rubbery polymers in more detail. Under crossed polarizers these samples are highly birefringent, and the color and intensity of light passing through the polarizer are changed when the sample is stretched. Moreover, the optical texture returns to its original state after the sample retracts to its initial dimension. Preliminary SAXS measurements on stretched samples indicate that the smectic layers orient parallel to the stretch direction and that the *d* spacing of these smectic layers remains the same before and after stretching.

Miscibility between the LCP and PS blocks was an unexpected issue in these systems, as siloxanes are highly immiscible with polystyrene, and the liquid crystallinity of the siloxane block was expected to *further* insure the immiscibility of the blocks. However, it should be noted that polystyrene is known to be miscible with polycarbonate derivatives and with PPO [32], which have aromatic, ester, and ether functional groups as do the mesogens in this study. In addition, we found that the small molecule analogue of mesogen A is an excellent plasticizer for polystyrene, lowering its T_g to 30°C in a 50/50 blend. This offers some explanation as to why the phase segregation appeared weak in some of the mesogen A containing block copolymers. Finally, there are examples of crystalline-amorphous polymer pairs which are miscible (PEO–PMMA) [33],

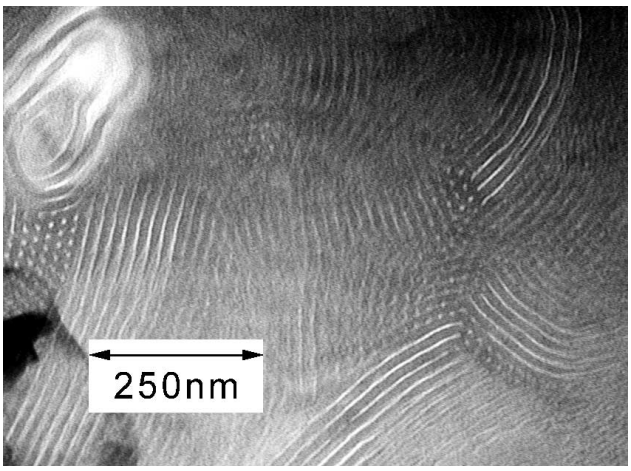

Fig. 8. TEM image of hexagonally packed LC cylinders, sample PS 12–LCPB 8. The polystyrene regions appear dark in this image due to the RuO_4 stain.

suggesting that certain LCP-amorphous polymer pairs may also be miscible despite the presence of liquid crystallinity in the LCP.

3.3. Mesogen B polymers: LC phase behavior and morphology

To introduce a higher degree of phase segregation, we designed mesogen B, which has a shorter spacer and a more rigid mesogen unit (see Fig. 2). A similar mesogen structure had been used before by our research group which gave strong segregation in PS–LC methacrylates [7], at relatively low LCP MWs (~8000). The length of the fully extended mesogen B was calculated to be 3.2 nm using the MOPAC molecular modeling package. This number is the same as the 3.2 nm smectic spacing measured in all the LC homopolymers by SAXS, and suggests that the phase structure could be S_A^*. This phase assignment is further supported by electro-optic switching experiments on mesogen B homopolymers, which resulted in electroclinic switching characteristic of the S_A^* phase.

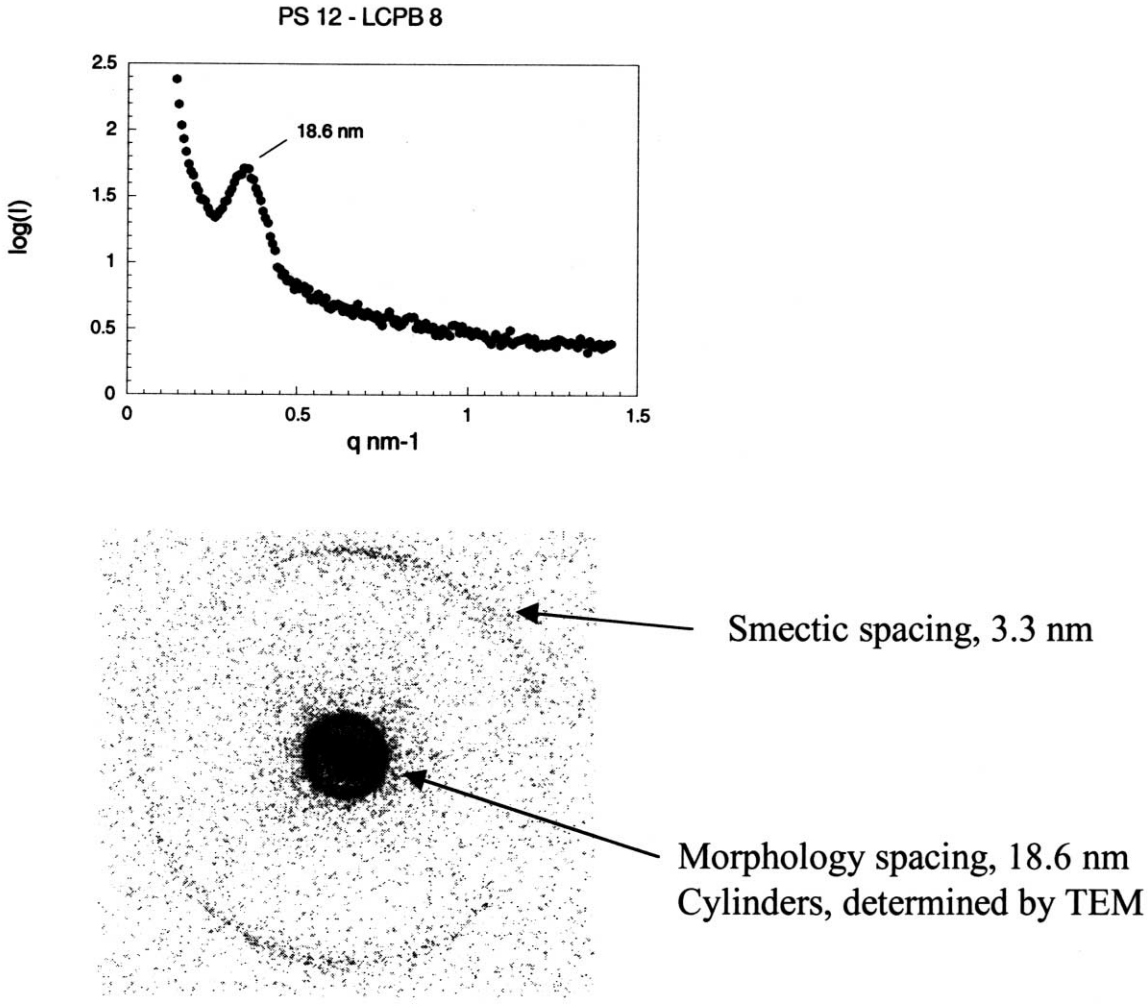

Fig. 9. 1-D and 2-D SAXS plots of PS 12–LCPB 8 after annealing the sample overnight at 110°C. The 2-D plot reveals that the mesogens are aligned along the axis of the LCP cylinders shown in Fig. 8. The orientation in this sample was induced from the solvent casting and annealing process.

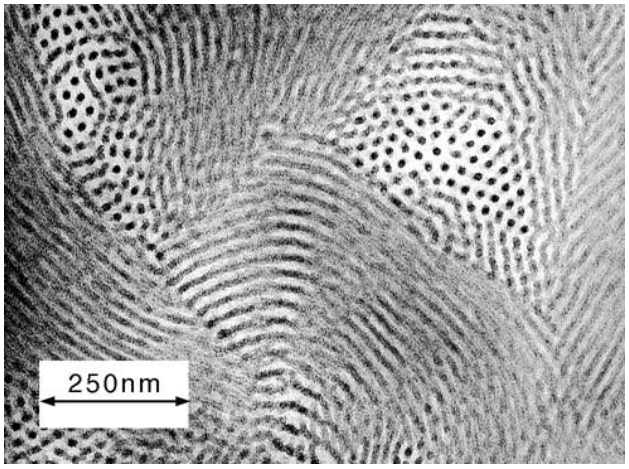

Fig. 10. TEM image of sample PS 14–LCPB 151. The hexagonally packed polystyrene cylinders appear dark in the TEM image due to the RuO_4 stain. Note that the phase boundaries are more distinct than the mesogen A analogue, PS 14–LCPA 132 (Fig. 7).

Two block copolymer samples were prepared with mesogen B, using the same block copolymer substrates as in PS 12–LCPA 8 and PS 14–LCPA 132. This gives a direct comparison of two PS–LCP block polymers that differ in the mesogen attached to the siloxane block.

The most remarkable difference between these two series of polymers is that the mesogen B containing polymers have a greater tendency to phase segregate into ordered morphologies. Whereas PS 12–LCPA 8 is phase mixed by all measures, PS 12–LCPB 8 is clearly phase segregated, with small liquid crystalline cylinders hexagonally packed in a polystyrene matrix, as shown in Fig. 8. The degree of mesogen substitution in both PS 12–LCPA 8 and PS 12–LCPB 8 polymers is close to 100%, indicating conclusively that mesogen B yields siloxane blocks that are less miscible with polystyrene than LCP siloxanes made with mesogen A.

Fig. 9 shows 1-D and 2-D SAXS scattering for PS 12–LCPB 8, and Fig. 8 shows a TEM image of the hexagonally packed LCP cylinder morphology. The 2-D SAXS pattern shows that the smectic layers are perpendicular to the cylinder axis. This orientation was not induced by shear, but by the slow solvent evaporation and the geometry of the film. The strongly segregated morphology was present prior to annealing, although the SAXS peak became more well defined with annealing at 110°C, and the cylinders became oriented in the film direction. A unique feature of these cylinders is their small diameter, ~6.0 nm as estimated from the TEM image. This constitutes an 'area fraction' of 0.19, which is much smaller than the theoretical value of 0.40 based on the volume fraction of the blocks. This reflects a general trend in both mesogen A and B block copolymers of the polystyrene regions appearing larger than expected in TEM, even when taking into account the density difference between the blocks (Polystyrene $\rho = 1.05$, LCPB 35 $\rho = 1.12$; measured by floatation in salt water). This observation is not unprecedented in PS–LCP systems stained with RuO_4 [31], and suggests that these regions may be physically swollen by the RuO_4 stain or that the interfacial region may be stained.

On the other side of the composition range, we have similar results. PS 14–LCPB 151 has a morphology of hexagonally packed polystyrene cylinders in a liquid crystalline matrix (Fig. 10). The toluene cast PS 14–LCPB 151 showed no Bragg reflection in SAXS; after annealing at 110°C, however, a first-order shoulder at 28.6 nm formed. In addition, the phase boundaries observed in the TEM image of PS 14–LCPB 151 are more distinct than in PS 14–LCPA 132, suggesting stronger phase segregation in the mesogen B containing block copolymer. Once again the polystyrene domains (cylinders, in this case) occupy a greater area fraction in the TEM image (0.17) than predicted theoretically from the block sizes (0.09). Table 7 summarizes the TEM and SAXS observations for mesogen B containing polymers.

This observation of polystyrene cylinders at high LCP weight fractions is unusual, as PS spheres would normally be expected in this composition range. However, similar observations were recently reported in PS–LCP systems containing an anzobenzene/cyanobiphenyl mesogen [32], and were attributed to enthalpic penalties associated with packing mesogens around spherical objects.

It should be noted that PS 14–LCPB 151 has a 99% substitution of mesogen groups, while PS 14–LCPA 132 has an 86% substitution of the mesogen groups. Therefore, the comparison between these samples is less satisfactory than in the case of PS 12–LCPA 8 and PS 12–LCPB 8, both of which have mesogen substitutions close to 100%.

The thermal properties of the polymers made with mesogen B appear in Table 8. The smectic clearing points and the siloxane T_g in the mesogen B polymers are both higher than those observed with mesogen A. Moreover, the smectic clearing points do not become depressed with decreasing

Table 7
SAXS peaks and TEM observations of polymers made w/mesogen B

Sample ID	Wt % LCP	SAXS smectic *d* spacing (nm)	SAXS morphology spacing (nm)	TEM morphology, spacing (nm)
LCPB 47	100	3.1	–	
PS 12–LCPB 8	41	3.3	18.0	LCP hex. packed cylinders 15.5 (D cyl. 6.3)
PS 14–LCPB 151	91	3.2	28.6, shoulder	PS hex. packed cylinders 25.2 (D cyl. 12.5)

Table 8
T_gs and smectic clearing points of polymers made with mesogen B. Thermal transitions are taken from the second or third heating scan at 20°C min^{-1}, except where indicated

Sample ID	Wt % LCP	PS T_g (°C)	LCP T_g (°C)	Smectic clearing pt (°C)	ΔH clearing J g^{-1} LCP
LCPB 47	100	–	− 3	153	4.246
PS 12–LCPB 8	41	89	− 6	175[a]	N/A[b]
PS 14–LCPB 151	91	82	4	157	3.828

[a] The clearing point was determined from temperature controlled SAXS, and coincided with the order–disorder transition.
[b] A distinct LC clearing point was not observed in DSC, even at lower heating rates (10°C min^{-1}).

LCP content, and the polystyrene block T_g is less depressed than in the case of mesogen A. In fact, the LC clearing point is 4°C higher in PS 14–LCPB 151 than in the homopolymer LCPB 47, likely due to the large molecular weight difference between the LCP blocks. In the context of TEM and SAXS data this thermal data further supports the claim that meosgen B containing block copolymers are more strongly phase segregated than polymers made with mesogen A. Also, the clearing point trends we observe for mesogen A and B are in agreement with previous observations of liquid crystals [33]. Specifically, increasing mesogen rigidity and aspect ratio leads to higher clearing points, and in the case of liquid crystalline polymers, to both higher T_gs and clearing points.

The lowest molecular weight sample, PS 12–LCPB 8, is weakly birefringent in OM and a clearing point is difficult to detect in both optical microscopy (OM) and DSC. However, a distinct smectic SAXS peak at 3.3 nm shows that this sample is liquid crystalline, as illustrated in Fig. 9. Moreover, this smectic SAXS peak disappears at ~175°C (measured using a SAXS hot-stage attachment), 22°C higher than the homopolymer, indicating that the smectic LC phase has been stabilized by confinement into small LC cylinders. This is the first reported stablization of an LC phase (relative to the homopolymer) by confinement within cylindrical domains; Mao et al. [9] and Yamada et al. [27] found that the cylindrical LC samples had higher clearing points than the lamellar samples, but comparable clearing points to the homopolymer analogues. In our case, the stabilization effect may be more pronounced because of the small diameter of the LC cyliners, ~6.0 nm. It is important to note that the order disorder transition temperature for sample PS 12–LCPB 8 corresponded with the LC clearing point as determined by SAXS, similar to observations reported for PS–LCP methacrylates with very similar molecular weights and mesogens [7]. The absence of a distinct LC clearing point in the DSC of PS 12–LCPB 8 may be due to this superposition of the clearing point and the ODT.

The physical properties of polymers made with mesogen B are quite different from mesogen A polymers, due to the higher T_g of the mesogen B siloxanes. While PS 14–LCPA 132 is elastomeric, PS 14–LCPB 151 forms a pliant tough material that is easy to bend but difficult to stretch. Thus, while the LCPB polymers have T_gs below room temperature (~0°C), this is not low enough to result in the elastomeric properties which were observed for LCP blocks with T_g ~ − 30°C.

4. Summary and conclusions

Two series of polystyrene-b-(liquid crystalline side-chain siloxane) diblock copolymers were synthesized using two structurally different mesogens, denoted A and B. In both instances, phase segregated morphologies and liquid crystalline properties were observed and evaluated. As the mesogen and block lengths were changed, four general classes of morphologies were observed: hexagonally packed LCP cylinders, alternating PS–LCP lamellae, weakly ordered PS cylinders, and hexagonally packed PS cylinders. Partial miscibility between polystyrene blocks and liquid crystalline siloxane blocks was not expected, but was observed in the case of the less rigid mesogen (mesogen A) with low molecular weight blocks. This is due to a favorable interaction between mesogen A and polystyrene. On the other hand, the more rigid mesogen resulted in stronger phase segregation between the LCP blocks and the PS blocks and in a higher a clearing point and T_g in the liquid crystal block.

Block copolymers with low T_g (< -25°C) and high weight fraction liquid crystal blocks (>0.8) formed liquid crystalline elastomers, with a morphology of weakly ordered PS cylinders in an LCP matrix. Current work is focused on extending these systems to PS–LCP–PS triblock copolymers to yield LCP thermoplastic elastomers with attractive mechanical and liquid crystalline properties.

Acknowledgements

The authors acknowledge the National Science Foundation Polymer Program for funding under Grant DMR-9526394. We also thank Professor Ned Thomas for the use of his ultracryomicrotome equipment and the MIT CMSE for use of their SAXS and TEM facilities.

References

[1] Adams J, Gronski W. Makromol Chem, Rapid Commun 1989;10:553–7.
[2] Zaschke B, Frank W, Fischer H, Schmutzler K, Arnold M. Polym Bull 1991;27:1–8.
[3] Percec V, Lee M. J Macromol Sci, Chem 1992;29:723.
[4] Chiellini EGG, Angeloni AS, Laus M, Bignozzi MC. Macromol Symp 1994;77:349–58.
[5] Yamada M, Iguchi T, Hirao A, Nakahama S, Watanabe J. Macromolecules 1995;28:50–58.
[6] Zheng WY, Hammond PT. Macromol Rapid Commun 1996;17:813–24.
[7] Zheng WY, Hammond PT. Macromolecules 1998;31:711–21.
[8] Omenat A, Hikmet RAM, Lub J, Van der Sluis P. Macromolecules 1996;29:6730–6.
[9] Mao G, Wang J, Clingman SR, Ober CK, Chen JT, Thomas EL. Macromolecules 1997;30:2556–67.
[10] Fischer HR. Prog Rubber Plastics Technol 1998;14:95–115.
[11] Zheng WY, Albalak R, Hammond PT. Macromolecules 1998;31:2686–9.
[12] Mao G, Wang J, Ober CK, Brehmer M, O'Rourke MJ, Thomas EL. Chem Mater 1998;10:1538–45.
[13] Zentel R, Reckert G, Bualek S. Makromol Chem 1989;190:2869–84.
[14] Finkelmann H, Kock H-J, Rehage G. Makromol Chem, Rapid Commun 1981;2:317–22.
[15] Shilov S, Gebhard E, Skupin H, Zentel R, Kremer F. Macromolecules 1999;32:1570–5.
[16] Meier W, Finkelmann H. Makromol Chem Rapid Commun 1990;11:599–605.
[17] Cooray NF, Kakimoto M, Imai Y, Suzuki Y. Polym J 1993;25:863–72.
[18] Suzuki TO. T Makromol Chem, Rapid Commun 1988;9:755–60.
[19] Finkelmann H, Rehage G. Makromol Chem, Rapid Commun 1980;1:31–34.
[20] Hsu CS, Shih LJ. Macromol Symp 1995;98:883–93.
[21] Moment A, Miranda R, Hammond PT. Macromol Rapid Commun 1998;19:573–9.
[22] Hempenius MA, Lammertink RG, Vansco JG. Macromolecules 1997;30:266–72.
[23] Saam JC, Gordon DJ, Lindsey S. Macromolecules 1970;3:1–4.
[24] Davies WG, Penarth, Elliot B, Markham, Blackwood N, Kendrick TC. Polymerization of Siloxanes, US Patent 3,481,898, 1969.
[25] Saam JC. Formation of Linear Siloxane Polymers. In: Ziegler JM, Fearon FWG, editors. Silicon-based polymer science: a comprehensive resource. Washington, DC: American Chemical Society, 1990. p. 71–90.
[26] Yamada M, Itoh T, Nakagawa R, Hirao A, Nakahama S, Watanabe J. Macromolecules 1998;32:282–9.
[27] Omenat A, Lub. J Chem Mater 1998;10:518–23.
[28] Fischer H, Poser S, Arnold M, Frank W. Macromolecules 1994;27:7133–8.
[29] Anthamatten M, Zheng WY, Hammond PT. Macromolecues 1999;32:4838–48.
[30] Shaw MT. J Appl Polym Sci 1974;18:449–72.
[31] Chow TS. Macromolecules 1990;23:333–7.
[32] Osuji CO, Chen JT, Mao G, Ober CK, Thomas EL. Polymer 2001 (in press).
[33] Gray GW. Relationship between chemical structure and properties for low molecular weight liquid crystals. In: Ciferri A, Krigbaum WR, Meyer RB, editors. Polymer liquid crystals. New York: Academic Press, 1982. p. 1–33.